Journal of Materials Chemistry A

Accepted Manuscript

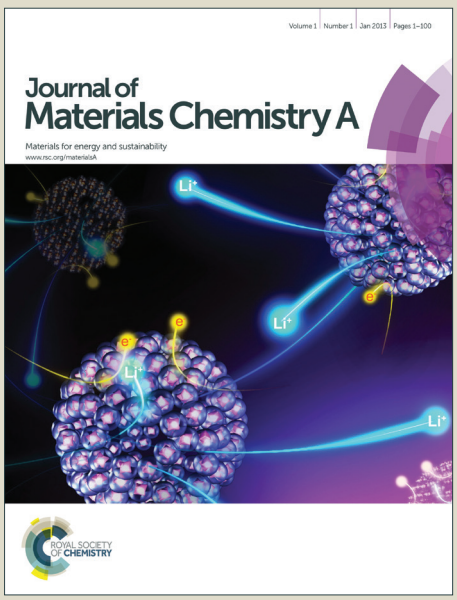

ROYAL SOCIETY OF CHEMISTRY

www.rsc.org/materialsA

Cite this: DOI: 10.1039/c0xx00000x

www.rsc.org/xxxxxx

ARTICLE TYPE

Fe_3O_4/PANI/*m*-SiO_2 as Robust Reactive Catalyst Supports for Noble Metal Nanoparticles with Improved Stability and Recyclability

Jie Han*, Song Lu, Chenjing Jin, Minggui Wang and Rong Guo*

Received (in XXX, XXX) Xth XXXXXXXXX 20XX, Accepted Xth XXXXXXXXX 20XX

DOI: 10.1039/b000000x

Developing catalysts with improved stability and efficiency is increasingly important for both economic and environmental reasons. Herein, Fe_3O_4/PANI/*m*-SiO_2 hybrid core/shell spheres have been successfully synthesized as novel and robust reactive catalyst supports to produce highly stable and recyclable noble metal nanocatalysts. Specifically, Fe_3O_4/PANI/*m*-SiO_2 hybrid core/shell spheres were firstly fabricated, followed by the addition of noble metal ions to initial the redox reaction between PANI and noble metal ions to give up noble metal nanoparticles on surfaces of PANI. The Fe_3O_4 core and mesoporous SiO_2 shell of Fe_3O_4/PANI/*m*-SiO_2 hybrid supports can significantly improve the recycling efficiency and greatly reinforce the stability of catalyst nanoparticles against coagulation, respectively. Various parameters, such as thickness of PANI coating and etching time of SiO_2 dense shell had been considered to optimize the catalyst supports. Furthermore, high stability and recyclability of Fe_3O_4/PANI/Au/*m*-SiO_2 hybrid catalysts involved in liquid phase reactions have been established, which implies their potential applications in field of catalysis.

Introduction

Noble metal nanoparticles with high surface areas have been well-recognized as promising nanocatalysts involved in liquid or gaseous reactions.[1-4] Therefore, much attention has been paid to the rational design and synthesis of noble metal nanoparticles with controllable size[5-7] and specific shape[8-16] due to their determining roles in catalytic activity. Although the obvious advantages of simple separation, reusability, and catalytic selectivity have been evidenced when compared with homogeneous catalysts,[17, 18] unsupported nanocatalysts tend to coagulate and therefore lose their initial catalytic activity and selectivity due to their high surface energies. As a result, supported noble metal nanoparticles have been demonstrated to reduce the surface energies of noble metal nanoparticles and then maintain or improve their stability and reusability in catalytic reactions. Typically, the supports for noble metal nanoparticles are activated carbon or metal oxides.[19-21] In recent years, the supports of interest for noble metal nanoparticles have shifted from activated carbon or metal oxide inorganic materials to polymers because of the merits of mild and simplified synthetic conditions and higher catalytic performances.[22]

Until now, many different polymers have been utilized to stabilize noble metal nanoparticles, which involve the most popular poly(vinylpyrrolidone) (PVP),[23-25] polystyrene derivatives[26] and others.[27-29] The choice of polymers is based on the fact that noble metal nanoparticles can be sized and shaped throughout the nucleation and growth processes through the interactions between the specific functional groups in polymers and noble metal nanoclusters. More recently, conducting polymers of polyaniline (PANI) have also been developed to act as superior supports for noble metal nanoparticles.[30-32] PANI, as one of the most intensively investigated conducing polymers, is unique due to their reversible acid/alkali doping/dedoping property, tunable chemical structures through redox and abundant functional groups in main chains.[33-35] Considering amine groups and benzene rings that coexisted in polymer chains can bind to certain metal atoms on the surface of nanoparticles, PANI and its derivatives have been extensively exploited to stabilize noble metal nanoparticles. Two strategies are normally applied to synthesize PANI-supported noble metal nanoparticles. Firstly, aniline monomers and noble metal ions are mixed to initial the redox reaction between them to produce PANI-supported noble metal nanoparticles. In this case, noble metal nanoparticles are typically embedded in polymer matrix. Although such composites show high stability, the dense organic coatings make it difficult for reactant molecules to reach buried active catalysts, thus showing low catalytic activity.[36] Secondly, PANI polymers and noble metal ions are mixed to initial the redox reaction between them to produce PANI-supported noble metal nanoparticles. Due to the redox reactions happens on surfaces of pre-designed PANI nanostructures, noble metal nanoparticles are typically supported on surfaces of polymer matrix. High catalytic activities can be evidenced because of the low pathway between reactant molecules and active catalysts, however, nanoparticles are inclined to coagulate during reaction processes due to lack of efficient isolation between nanoparticles, thus showing low stability and recyclability.[31, 37-39] Therefore, it remains a great challenge to synthesize PANI-supported noble metal nanoparticles with both improved stability and catalytic activity.

Herein, Fe_3O_4/PANI/*m*-SiO_2 hybrid core/shell spheres have been developed as novel and robust reactive catalyst supports to produce highly stable and efficient noble metal catalysts. Firstly, a thin layer of PANI polymer is coated on surfaces of Fe_3O_4 spheres, followed by another coating of SiO_2. Using the reported "surface-protected etching" strategy,[40-42] mesoporous SiO_2 shells with nanochannels can be achieved, realizing the transformation of Fe_3O_4/PANI/SiO_2 into Fe_3O_4/PANI/*m*-SiO_2 hybrid core/shell spheres. Finally, using the redox activity between PANI and various noble metal ions (including Au, Ag, and Pd),[43] Fe_3O_4/PANI/noble metal nanoparticle/*m*-SiO_2 hybrid core/shell spheres can be fabricated after addition of noble metal ions into Fe_3O_4/PANI/*m*-SiO_2 reactive supports. The introduction of *m*-SiO_2 outer layer shows multifunctionalities: 1) As for synthesis, channels of mesoporous SiO_2 outer layers act as nanoreactors to allow noble metal ions to encounter PANI, meanwhile, control the size of noble metal nanoparticles during redox reactions and stabilize noble metal nanoparticles against coalescence afterwards; 2) In respect to catalysis, channels of *m*-SiO_2 outer layers let reactant molecules to reach active catalysts without blocking, leading to high catalytic activity. Furthermore, mesoporous SiO_2 outer layers together with noble metal nanoparticles reduce the possibility of polymers dissolution in reaction medium (especially in catalytic reactions with organic solvents), leaving less impurity in reaction medium after magnetic separation of catalysts. Typically, Fe_3O_4/PANI/Au/*m*-SiO_2 hybrid core/shell spheres were synthesized and their catalytic activities were examined by choosing the model catalysis reaction involving reduction of 4-nitrophenol (4-NP) to 4-aminophenol (4-AP) in the presence of $NaBH_4$. Superior catalytic performances with high stability and recyclability have been revealed, which indicate their potential applications in field of catalysis.

Experimental

Materials

Aniline was distilled under reduced pressure before use. All other reagents were of analytical grade and used without further purification. The water used in this study was deionized by milli-Q Plus system (Millipore, France), having 18.2 MΩ electrical resistivity.

Synthesis of Fe_3O_4 Spheres

The magnetic Fe_3O_4 spheres were prepared through a solvothermal reaction.[44] Briefly, $FeCl_3 \cdot 6H_2O$ (0.54 g), sodiumacrylate (1.5 g), and sodium acetate (1.5 g) were dissolved in ethylene glycol (20 mL) under vigorous magnetic stirring for more than 2 h at room temperature. The obtained yellow solution was transferred to a Teflon-lined stainless steel autoclave. The autoclave was then heated in an electric oven at 200 °C for 10 h. and then allowed to cool down to room temperature. The black products can be collected by magnetic separation. Finally, the products were washed with deionized water and ethanol for three times, respectively, and then dried at 60 °C for 12 h.

Synthesis of Fe_3O_4/PANI Core/Shell Spheres

In a typical synthesis, 20 mg as-prepared Fe_3O_4 were dispersed in 25 ml deionized water, followed by the addition of 100 mg PVP (K-30, Mw~5000). After sonication for 30 min, 12 mg aniline and 50 μL concentrated HCl (36-38 wt%) were added into the mixture and the solution was stirred for 12 h at room temperature. The sonicator was operated at 42 kHz using a Branson 5510E-DTH apparatus. Then, 20 ml deionized water was added and the mixture was further sonicated for 1 h at room temperature. After 1 h, an aqueous solution of ammonium peroxydisulfate (APS) oxidant (0.6 g APS in 20 mL deionized water) was added to start the oxidative polymerization under ultrasonic irradiation. The reaction was allowed to proceed for 2 h at room temperature. Finally, the products were magnetic separated and washed by deionized water and ethanol for three times, respectively, and then dispersed in 4 mL deionized water.

Synthesis of Fe_3O_4/PANI/SiO_2 Core/Shell Spheres

Typically, the above-mentioned Fe_3O_4@PANI colloidal solution (1 mL) was mixed with 9 mL PVP solution containing 0.2 g PVP (Mw = 55000). The mixture was sonicated for 20 min to allow adequate polymer to adsorb to the particle surface. The mixture was magnetic separated subsequently to remove the unbound polymer and then dispersed in a mixture of 20 mL ethanol, 2.5 mL deionized water, 1 mL aqueous ammonia (25-28 wt%) After 5 min ultrasonic treatment to disperse nanoparticles, 200 μL tetraethoxysilane (TEOS) was injected and the reaction was allowed to proceed for 12 h at room temperature under continuous mechanical stirring. The resultant Fe_3O_4/PANI/SiO_2 products were separated and collected with a magnet, followed by washing with deionized water and ethanol for three times, respectively, and then dried in a vacuum at 60 °C for 24 h.

Synthesis of Fe_3O_4/PANI/*m*-SiO_2 Core/Shell Spheres

The "surface-protected etching" strategy was applied to transform SiO_2 shells from dense into mesoporpous structures, realizing the successful transformation of Fe_3O_4/PANI/SiO_2 into Fe_3O_4/PANI/*m*-SiO_2 core/shell spheres. Typically, the above obtained Fe_3O_4/PANI/SiO_2 core/shell spheres were redispersed in 20 mL PVP solution containing 1 g PVP (K-25, Mw = 24000) under sonication. The solution was refluxed at 100 °C for 4 h and then cooled down to room temperature naturally. Then, NaOH aqueous solution (1 mL with concentration of 0.01 g mL^{-1}) was injected into the system to start the etching. After etching for 10 min, the mixture was magnetic separated instantly and the product was washed with deionized water three times, and then dispersed in 1 mL deionized water for further use.

Synthesis of Fe_3O_4/PANI/Au/m-SiO_2 Core/Shell Spheres

Typically, Fe_3O_4/PANI/m-SiO_2 colloiodal solution (0.5 mL) was redispersed in 9.5 mL deionized water. The mixture was maintained at 0 °C for 10 min, and then 50 μL $HAuCl_4$ aqueous solution (0.1 mol L^{-1}) was added to the above mixture. The resulting solution was shook for 10 s to ensure complete mixing and then the reaction was allowed to proceed without stirring for 1 h at 0 °C. Finally, the resultant Fe_3O_4/PANI/Au/*m*-SiO_2 products were separated and collected with a magnet. After washing with deionized water three times, the resulting solution was then dialyzed to remove any remaining $HAuCl_4$ in fresh deionized water every 8 h for 2 d. The particles were finally dispersed in 1 mL deionized water for catalysis. The Au concentration in solution was determined on a PerkinElmer Elan DRC-e inductively coupled plasma mass spectrometer (ICP-MS).

The mass fraction of Au nanoparticles to the quality of catalyst supports is up to 1.1%.

Catalytic Experiments

The reduction of 4-NP by $NaBH_4$ was chosen as a model reaction for testing efficiency of the catalysts. Typically, aqueous solution of $NaBH_4$ (3.0 mL, 0.015 mol L^{-1}) was mixed with aqueous 4-NP solution (5.1 mL, 0. 2 mmol L^{-1}), leading a color change from light yellow to yellow-green. Then, 0.9 mL Fe_3O_4/PANI/Au/*m*-SiO_2 colloidal solution as catalysts was added to initial the catalytic reaction. The progress of the conversion of 4-NP to 4-AP was then monitored via the Uv-vis spectroscopy by recording the time-dependent absorbance spectra of the reaction mixture in a scanning range of 200-600 nm at ambient temperature.

Characterization

Morphologies were examined by a transmission electron microscope (TEM, Tecnai-12 Philip Apparatus Co., USA). The Uv-vis spectra (UV-2501, Shimadzu Corporation, Japan) of samples were measured in the range between 200 and 600 nm. N_2 adsorption-desorption measurements were conducted using Thermo Sorptomatic 1990 by N_2 physisorption at 77 K. The as-calcined samples were out gassed for 4 h at 250 ºC under vacuum ($p<10^{-2}$ Pa) in the degas port of the sorption analyzer. The BET specific surface areas of samples were evaluated using adsorption data in a relative pressure range from 0.05 to 0.25. The pore size distributions were calculated from the adsorption branch of the isotherm using the thermodynamic-based Barrett-Joyner-Halenda (BJH) method. The metal ion concentration was measured by inductively coupled plasma atomic emission spectroscopy (ICP-AES) on an Optima7300 DV (Perkin Elmer). Gas chromatography (GC) analysis were performed on an Agilent DB-1 GC-FID system equipped with a 100 % dimethyl polysiloxane capillary column (length: 30 m, ID: 0.25 μm, film thickness: 0.25 μm). The GC yield was obtained from the calibration curve.

Results and discussion

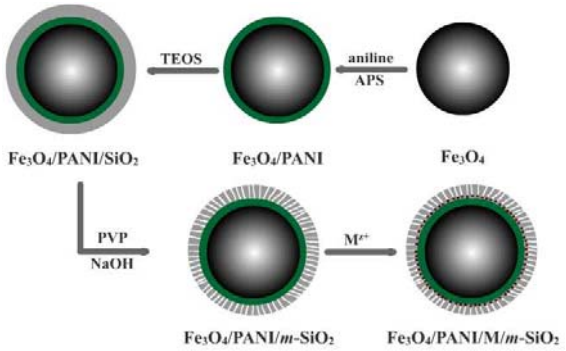

Scheme 1 Schematic illustration for the formation of Fe_3O_4/PANI/noble metal nanoparticle/*m*-SiO_2 core/shell spheres.

In order to improve the recyclability, superparamagnetic Fe_3O_4 spheres were incorporated as magnetic cores.[42, 44, 45] Scheme 1 outlines the general procedures for PANI-supported and mesoporous silica-protected magnetic noble metal nanocatalysts. Firstly, the reactive polymers of PANI are coated on surfaces of Fe_3O_4 spheres through chemical oxidation polymerization route, leading to the formation of Fe_3O_4/PANI core/shell spheres. Secondly, another layer of silica is coated on Fe_3O_4/PANI surfaces, followed by the "surface-protected etching" strategy for making mesoporous silica shell, resulting in Fe_3O_4/PANI/*m*-SiO_2 hybrid core/shell spheres. Finally, the simple introduction of noble metal ions into colloids solution of Fe_3O_4/PANI/*m*-SiO_2 reactive supports can produce Fe_3O_4/PANI/noble metal nanoparticle/*m*-SiO_2 hybrid core/shell spheres, where noble metal nanoparticles are formed on surfaces of PANI polymers.

Fe_3O_4/PANI/*m*-SiO_2 Reactive Catalyst Supports

It is found that PANI polymers are hard to coat on surfaces of Fe_3O_4 cores due to the incompatibility nature of those two materials. In order to realize the uniform coating of PANI on surfaces of Fe_3O_4 particles, sodium acrylate-modification of negetively charged Fe_3O_4 spheres, which can introduce the static intereactions with PANI, are chosen. Besides, ultrasonication treatment should be applied to avoid coagulation during polymerization reactions. Figure 1a shows as-formed Fe_3O_4 spheres with an average size of 400 nm. Figure 1b illustrates the typical TEM image of Fe_3O_4/PANI core/shell spheres with thin polymer coating, where rough surfaces with prominences can be evidenced. Clearly observation of the surface of a single particle (inset in Figure 1b) reveals the incontinuous PANI coating. With polymerization reaction time prolonging to 2.5 and 3 h, the incontinuous PANI coating becomes continuous (insets in Figures 1b-d), and the average thickness of PANI coating on surfaces of Fe_3O_4 particles increases to 27 nm (Figure 1c) and 34 nm (Figure 1d), respectively. In addition, it is found that further increase in reaction time leads to interconnected Fe_3O_4/PANI core/shell spheres, which is not suitable for further coating processes.

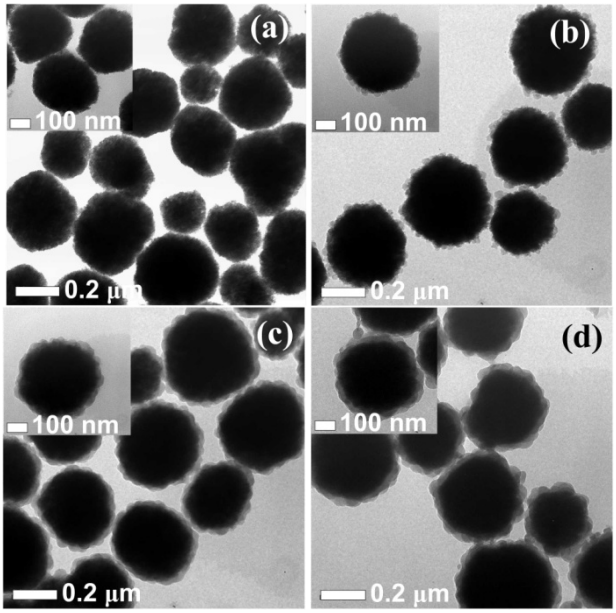

Fig. 1 TEM images of (a) Fe_3O_4 spheres and (b-d) Fe_3O_4/PANI core/shell spheres synthesized at different reaction time (h): (b) 2, (c) 2.5, and (d) 3.

The following step is to coat mesoporous SiO_2 shells on Fe_3O_4/PANI core/shell spheres. The most popular way for making mesoporous SiO_2 is assisted by cationic surfactant CTAB.[46-49] However, it does not work in our case. Because PANI

is normally positively charged, the addition of CTAB can significantly destabilize Fe_3O_4/PANI core/shell colloids and apparent precipitation of Fe_3O_4/PANI core/shell colloids caused by coagulation can be seen. Fortunately, "surface-protected etching" strategy as developed by Yin et. al.[50] can be applied to construct mesoporous SiO_2 shells derived from dense SiO_2 coating. Firstly, Fe_3O_4/PANI/SiO_2 core/shell spheres can be formed by adopting the well-known Stöber method using ethanol/H_2O mixed solvents, followed by NaOH treatment to selective dissolve of dense SiO_2 shells in the presence of PVP, realizing the transformation of SiO_2 shells from dense into mesoporous structures.

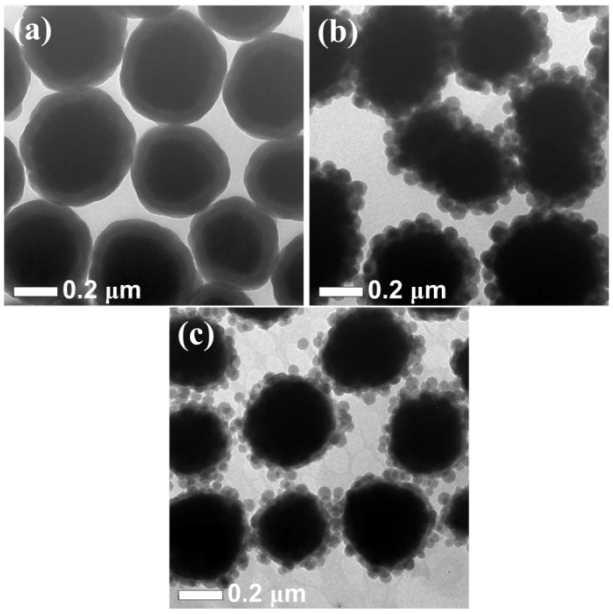

Fig. 2 (a-c) TEM images of Fe_3O_4/PANI/SiO_2 core/shell spheres using Fe_3O_4/PANI with increasing PANI coating as templates as given in Figure 1: (a) Figure 1b, (b) Figure 1c, and (c) Figure 1d.

Before coating of dense SiO_2 using Stöber method, PVP is always used to modify surfaces of colloid cores to ensure selective formation of SiO_2 on desired cores.[51] As seen in Figure 2a, uniform and smooth SiO_2 coating (50 nm in SiO_2 shell thickness) can be achieved when Fe_3O_4/PANI core/shell spheres with thin and incontinuous PANI coating (Figure 1b) are chosen. If Fe_3O_4/PANI core/shell spheres with thick and continuous PANI coating (27 nm in PANI shell thickness, Figure 1c) are applied, numerous interconnected SiO_2 nanospheres (80 nm in diameter) rooted on surfaces of Fe_3O_4/PANI core/shell spheres can be evidenced (Figure 2b). When choosing Fe_3O_4/PANI core/shell spheres with PANI shell thickness of 34 nm (Figure 1d), some individual SiO_2 nanospheres can be seen in addition to numerous interconnected SiO_2 nanospheres rooted on surfaces of Fe_3O_4/PANI core/shell spheres (Figure 2c). Results show that smooth and intact SiO_2 coating on surfaces of Fe_3O_4/PANI core/shell spheres only can be achieved with thin and incontinuous PANI coating. For comparison, Fe_3O_4 spheres without PANI coating (Figure 1a) are also used for SiO_2 coating using identical conditions, smooth and continuous SiO_2 coating on surfaces of Fe_3O_4 that is similar to Figure 2a can be observed. Without PANI coating on Fe_3O_4 surfaces, PVP can be adsorbed well on surfaces of Fe_3O_4, which provides favourable environments for hydrolysis of TEOS on PVP-modified Fe_3O_4 surfaces, leading to uniform SiO_2 coating on Fe_3O_4. When PANI is fragmentarily coated on Fe_3O_4 surfaces, PVP also can be selectively adsorbed on exposed Fe_3O_4 surfaces, and hydrolysis of TEOS on such regions leading to primary SiO_2, followed by continuous growth resulting in bridging adjacent SiO_2 particles to form continuous SiO_2 shells on Fe_3O_4 surfaces (Figure 2a). If Fe_3O_4 surfaces are mostly covered by PANI, less PVP can be penetrated and adsorbed on Fe_3O_4 surfaces. As a result, primary formed SiO_2 is less, and continuous hydrolysis of TEOS leading to interconnected SiO_2 particles on surfaces of Fe_3O_4. As the successful surface-modification is the key for uniform SiO_2 coating, it is hinted that PVP works well on hydrophilic surfaces of Fe_3O_4, whereas it is weakened on hydrophobic surfaces of PANI, which may result in the structure differences in SiO_2 coating.

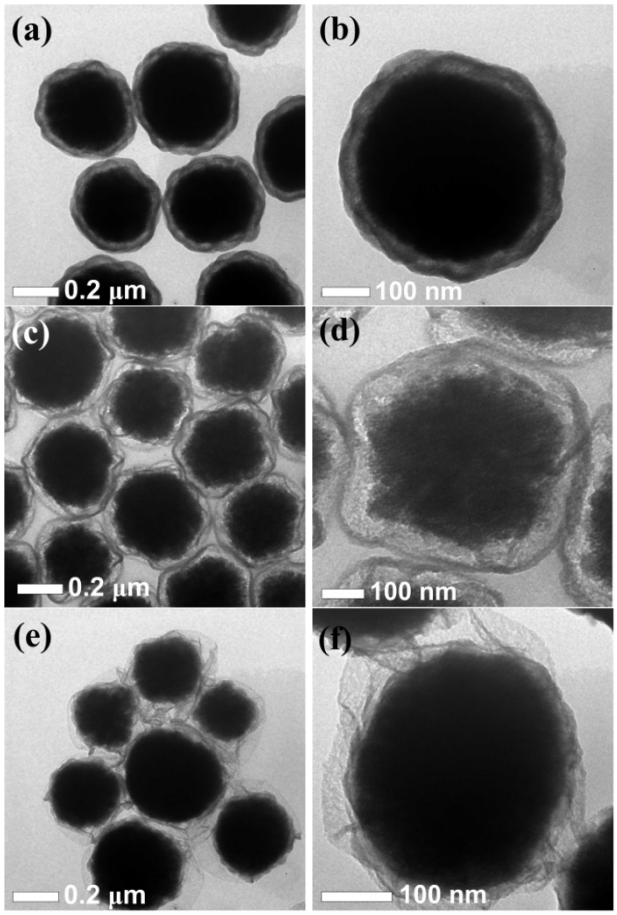

Fig. 3 (a-f) TEM images of Fe_3O_4/PANI/*m*-SiO_2 core/shell spheres using Fe_3O_4/PANI/SiO_2 core/shell spheres (Figure 3a) through "surface-protected etching" process at different etching times (min): (a, b) 5, (c, d) 10, and (e, f) 20.

Fe_3O_4/PANI/SiO_2 core/shell spheres with continuous and smooth SiO_2 coating (Figure 2a) are then chosen for further treatment due to its intact SiO_2 shell structures. Figures 3a, b show the TEM images of Fe_3O_4/PANI/*m*-SiO_2 core/shell spheres after "surface-protected etching" treatment of Fe_3O_4/PANI/SiO_2 core/shell spheres at etching time of 5 min. Dense SiO_2 shells have been successfully transformed into mesoporous structures. When the etching time increases to 10 min, although the surface

distortion can be clearly observed as compared with their original structure in Figure 2b, the porous frameworks of SiO_2 shells are believed to be left because all the Fe_3O_4/PANI cores are found to be concentrically positioned inside SiO_2 shells (Figures 3c, d). If the etching time further extends to 20 min, the most SiO_2 frameworks collapse (Figure 3e) and only thin and crapy SiO_2 shells are left on surfaces of Fe_3O_4/PANI cores (Figure 3f). If the etching time exceeds 30 min, SiO_2 shells are completely removed. Thereafter, Fe_3O_4/PANI/*m*-SiO_2 core/shell spheres as given in Figures 3a-d are selected as potential reactive catalyst supports for noble metal nanoparticles due to their porous and intact SiO_2 shells. N_2 adsorption-desorption measurements are then applied to disclose the surface properties (Figure 4a). The BET (Brunauer-Emmett-Teller) surface areas of Fe_3O_4/PANI/*m*-SiO_2 core/shell spheres in Figures 3a and c are 153.6 and 102.2 $m^2 g^{-1}$, respectively, whereas that of the original Fe_3O_4/PANI/SiO_2 core/shell spheres is 61.6 $m^2 g^{-1}$. The average BJH pore diameters calculated from the desorption branch of the isotherm are shown in Figure 4b, where significant increase in pore size with etching time can be clearly evidenced, which agrees with their corresponding TEM images.

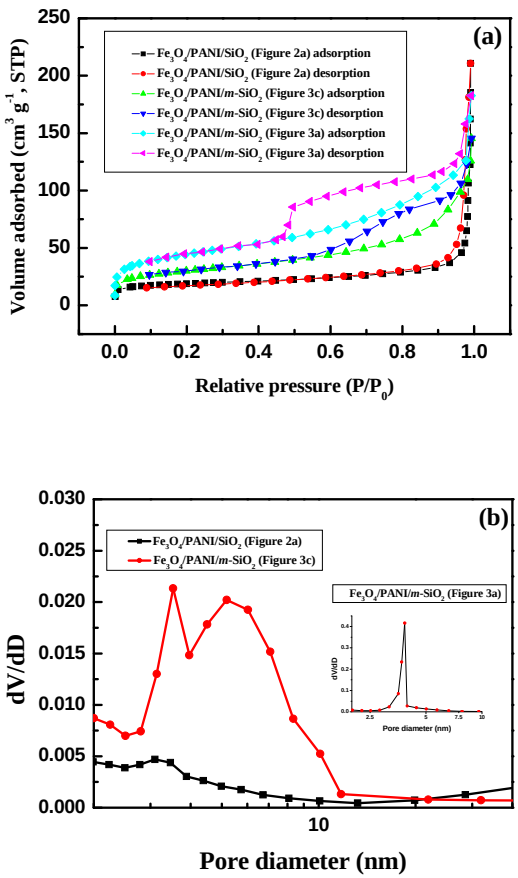

Fig. 4 (a) N_2 adsorption-desorption isotherms of Fe_3O_4/PANI/SiO_2 and Fe_3O_4/PANI/*m*-SiO_2 core/shell spheres and (b) their corresponding pore size distribution.

Fe_3O_4/PANI/Au/*m*-SiO_2 Catalysts

The last step is to introduce noble metal nanoparticles with catalytic centers in Fe_3O_4/PANI/*m*-SiO_2 catalyst supports. It is well-documented that PANI possesses several intrinsic oxidation states: the emeraldine base form is an intermediate oxidation state between pernigraniline, which is fully oxidized, and leucoemeraldine, which is fully reduced.[52] Several groups have discovered that the emeraldine base form of PANI can reduce noble metal ions into metallic states, whereas the emeraldine base form of PANI is oxidized into pernigraniline.[32, 37-39, 53-55] Herein, when $HAuCl_4$ aqueous solution is added into Fe_3O_4/PANI/*m*-SiO_2 (etching time = 5 min, Figure 3a) colloidal solution, Au nanoparticles with an average size of 6 nm (which is larger than pore size of porous SiO_2 shells) supported on surfaces of PANI can be evidenced (Figure 5a). The typical magnified TEM image of a single sphere as given in Figure 5b disclose that Au nanoparticles are exclusively supported on surfaces of PANI. Results confirm that Au nanoparticles are *in-situ* formed on surfaces of PANI. When using Fe_3O_4/PANI/*m*-SiO_2 with large pore size (etching time = 10 min, Figure 3c), most Au nanoparticles ranging in size from 5 to 10 nm (which is similar to pore size of porous SiO_2 shells) are located on surfaces of Fe_3O_4/PANI cores, and there are seldom in porous SiO_2 channels (Figures 5c and d).

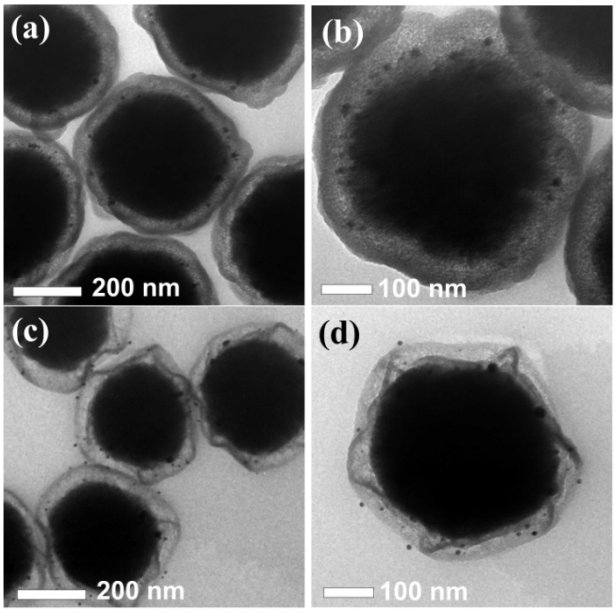

Fig. 5 TEM images of Fe_3O_4/PANI/Au/*m*-SiO_2 core/shell spheres using Fe_3O_4/PANI//*m*-SiO_2 core/shell spheres as reactive templates as given in (a, b) Figure 3a and (c, d) Figure 3c.

The stability of such catalysts is then highlighted. It is found that Au nanoparticles embedded in Fe_3O_4/PANI/*m*-SiO_2 catalyst supports are highly stable over time and mechanical agitation. For example, the synthesized Fe_3O_4/PANI/Au/*m*-SiO_2 catalysts shown in Figure 5c can be stable without obvious aggregation for more than four months (Figure S1), which undoubtedly evidence their high stability. For comparison, Fe_3O_4/PANI/Au hybrids are synthesized where Fe_3O_4/PANI without mesoporous SiO_2 shells are used as reactive supports for Au nanoparticles. It is not surprising that smaller Au nanoparticles (~ 2 nm in diameter) are found on surfaces of PANI because of increased nuclei centers and fast reaction rates in the absence of SiO_2 shells. However, it is found that obvious aggregation of Au nanoparticles on surfaces

of PANI can be evidenced when Fe_3O_4/PANI/Au colloids are stored for one week (Figure S2). Therefore, it is believed that the introduction of mesoporous SiO_2 shells can significantly reinforce the stability of catalyst nanoparticles against coagulation. It is anticipated that other noble metal nanoparticles, such as Ag, Pd and Pt, also can be *in situ* formed on PANI surfaces of Fe_3O_4/PANI/*m*-SiO_2 hybrid supports by a similar synthetic strategy due to the redox ability of PANI towards other noble metal ions,[38, 43, 56] which is currently under way. Therefore, it is believed that this is a controllable and energetic route to magnetic Fe_3O_4/PANI/noble metal nanoparticle/*m*-SiO_2 hybrid catalysts.

Catalytic Performances

It is interesting to disclose the catalytic performances of as-formed Fe_3O_4/PANI/Au/*m*-SiO_2 hybrid core/shell spheres due to their recyclability and improved stability. A model reaction of liquid phase reduction of 4-NP to 4-AP in the presence of $NaBH_4$ is chosen to evaluate the catalytic performances of Fe_3O_4/PANI/Au/*m*-SiO_2 hybrid core/shell spheres. Time-dependent adsorption spectra of this reaction mixture show the disappearance of the peak at 400 nm that is accompanied by a gradual development of a new peak at 300 nm corresponding to the formation of 4-AP (Figure 6a). The formation of exclusive 4-AP product has been further confirmed by ^{1}H NMR and GC analysis. Since excess $NaBH_4$ is present in the reaction solution and the reduction of 4-NP by $NaBH_4$ is negligible in the absence of Au nanoparticles (Figure 6b), the reaction can be considered pseudo-first-order with respect to the concentration of 4-NP. Before catalytic test, the adsorption equilibrium of 4-NP on surfaces of catalysts should be studied. It is found that the adsorption can reach equilibrium within 10 min. In addition, 11 % and 4% of 4-NP can be adsorbed on surfaces of Fe_3O_4/PANI/Au/*m*-SiO_2 and Fe_3O_4/PANI/Au hybrids core/shell spheres, respectively. Results indicate the superior adsorption ability of mesoporous silica shell.

The reduction of 4-NP into 4-AP using Fe_3O_4/PANI/Au/*m*-SiO_2 catalysts was completely finished within 40 min, and the colour change of bright yellow to colourless was observed. A linear relation of $\ln(c_t/c_0)$ versus time, where c_t and c_0 are 4-NP concentrations at time t and 0, respectively, is observed for Fe_3O_4/PANI/Au/*m*-SiO_2 hybrid core/shell catalysts, indicating that the reduction reaction can be considered as a pseudo-first-order reaction, and the rate constant is estimated to be 0.025 min^{-1} (Figure 6b). In the control experiments, Fe_3O_4 and Fe_3O_4/PANI colloids instead of Fe_3O_4/PANI/Au/*m*-SiO_2 hybrids show no catalytic activity in the same catalytic reactions, from which we can ascribe the catalytic activity from Au nanoparticles. For comparison, freshly prepared Fe_3O_4/PANI/Au spheres without porous SiO_2 shells (Figure S2a and b) are also used as catalysts and the rate constant is estimated to be 0.055 min^{-1} (Figure 6b), which is larger than that of Fe_3O_4/PANI/Au/*m*-SiO_2 hybrid core/shell catalysts. Results are reasonable because Fe_3O_4/PANI/Au spheres have smaller Au size and the absence of porous SiO_2 shells also in favour of mass transfer that contributes to the improved catalytic efficiency. However, Fe_3O_4/PANI/Au spheres will completely lose catalytic efficiency when they are stored for one week due to coagulation of Au nanoparticles (Figure S2c and d). As for Fe_3O_4/PANI/Au/*m*-SiO_2 hybrid core/shell catalysts, the catalytic efficiency almost unchanged when they are stored for more than four months due to their high stability. In addition, the supports of PANI in Fe_3O_4/PANI/Au/*m*-SiO_2 hybrids are believed to contribute to improved catalytic efficiency of Au catalysts because the intrinsic conducting nature of PANI favours electron transfer of catalysts.[57, 58] However, the complete removal of PANI through selective dissolution or calcinations will lead to aggregated Au nanoparticles as Au nanoparticles are stabilized by both mesoporous SiO_2 and PANI, which makes the control experiment to disclose their catalytic function unavailable at this stage.

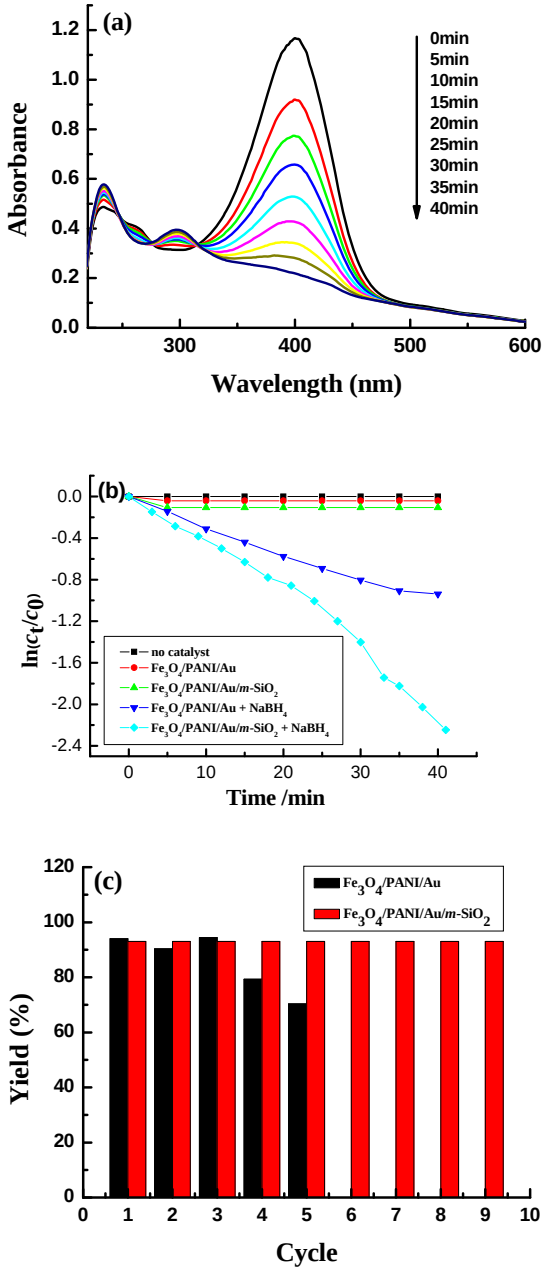

Fig. 6 (a) Uv-vis spectra showing gradual reduction of 4-NP with Fe_3O_4/PANI/Au/*m*-SiO_2 core/shell spheres in the first run. (b) Plot of $\ln(c_t/c_0)$ of 4-NP against time. (c) Synthesis yield of 4-AP in the nine

successive reactions with Fe_3O_4/PANI/Au and Fe_3O_4/PANI/Au/*m*-SiO_2 core/shell spheres.

We have also investigated the activities of Fe_3O_4/PANI/Au/*m*-SiO_2 hybrid core/shell catalysts towards the reduction of 3-NP, 2-NP, and other nitroaromatic compounds of 4-nitroaniline (4-NA), 3-NA and 2-NA (Figure S3). The reaction rates have been observed to follow the order: 4-NP > 2-NP > 3-NP, and the same order has been found for NA. The conclusions are consistent with reported results.[59]

Although recyclability is usually regarded as an advantage of heterogeneous catalysts, their practical applications in liquid-phase reactions still suffer from reduced catalytic activity resulting from nanoparticle coagulation. When freshly prepared Fe_3O_4/PANI/Au spheres without porous SiO_2 shells are repeated in such catalytic reactions, the apparent decrease in catalytic efficiency and complete loss in catalytic activity after fifth runs can be found as given in Figure 6c. Checking the TEM image of Fe_3O_4/PANI/Au spheres after five runs reveals the obvious aggregation of Au nanoparticles (Figure S4). If Fe_3O_4/PANI/Au/*m*-SiO_2 hybrid core/shell catalysts are conducted in repeated catalytic reactions, the catalytic efficiency remained at least within nine runs. Although the magnetic Fe_3O_4 cores have been detected with 1.4 % in weight loss after the first run, there is undetectable loss in Au catalysts as proved by ICP-AES analysis. Besides, no obvious Au nanoparticle coagulation can be evidenced as confirmed from TEM image, which undoubtedly proves high reusability of Fe_3O_4/PANI/Au/*m*-SiO_2 hybrid core/shell catalysts. Furthermore, catalysts can be recovered through simple magnetic separation (Figure S5a). It is also observed that Fe_3O_4/PANI/Au/*m*-SiO_2 catalysts preserve high colloidal stability after removal of magnet (Figure S5b). As a result, although the catalytic efficiency of Fe_3O_4/PANI/Au/*m*-SiO_2 hybrids is moderate,[60] their superior stability and recyclability make the developed synthesis strategy useful for the design of active catalytic nanoreactors and potential applications in field of catalysis.

Conclusions

Fe_3O_4/PANI/*m*-SiO_2 hybrid core/shell spheres as novel and robust reactive catalyst supports have been fabricated. Utilization the redox activity of PANI towards Au ions, Fe_3O_4/PANI/Au/*m*-SiO_2 hybrid core/shell spheres as highly stable and efficient noble metal catalysts can be fabricated. The introduction of porous SiO_2 shells not only acts as barriers to control catalyst nucleation and then avoid catalyst coagulation, but also acts as channels for mass transfer of reagents. Their superior stability and simple recyclability involved in a model liquid phase reaction have been demonstrated, which indicate their potential applications as efficient heterogeneous catalysts involved in liquid-phase catalysis. Because of the adjustability of both reactive cores (conducting polymers) and nanocatalysts (noble metal nanoparticles), which has been shown by our preliminary study, the proposed synthetic strategy is believed to construct recyclable and stable efficient supported noble metal nanocatalysts with tunable functionalities and therefore potential catalytic applications.

Acknowledgements

The authors gratefully acknowledge financial support from the National Natural Science Foundation of China (No. 21273004, 20903079 and 21073156), Research Fund for the Doctoral Program of Higher Education of China (20113250110007), and the Priority Academic Program Development of Jiangsu Higher Education Institutions. We would also like to acknowledge the technical support received at the Testing Center of Yangzhou University.

Notes and references

School of Chemistry and Chemical Engineering, Yangzhou University, Yangzhou, 225002, Jiangsu, P. R. China Fax: 86 514 8797 5219; Tel: 86 514 8797 5219; E-mail: hanjie@yzu.edu.cn; guorong@yzu.edu.cn

† Electronic Supplementary Information (ESI) available: Additional TEM images of Fe_3O_4/PANI/Au and Fe_3O_4/PANI/Au/*m*-SiO_2 catalysts, catalytic activities towards other nitroaromatic compounds, and optical images of Fe_3O_4/PANI/Au/*m*-SiO_2 catalysts before and after removal of magnet. See DOI: 10.1039/b000000x/

1 X. Fang, Z. Liu, M. Hsieh, M. Chen, P. Liu, C. Chen, N. Zheng, *ACS Nano*, **2012**, *6*, 4434-4444.
2 P. Hervés, M. Pérez-Lorenzo, L. M. Liz-Marzán, J. Dzubiella, Y. Lu, M. Ballauff, *Chem. Soc. Rev.*, **2012**, *41*, 5577-5587.
3 Y. Liu, J. Goebl, Y. Yin, *Chem. Soc. Rev.*, **2013**, *42*, 2610-2653.
4 L. Hou, Q. Zhang, F. Jérôme, D. Duprez, F. Can, X. Courtois, H. Zhang, S. Royer, *ChemCatChem*, **2013**, *5*, 1978-1988.
5 N. V. Izarova, M. T. Pope, U. Kortz, *Angew. Chem. Int. Ed.*, **2012**, *38*, 9492-9510.
6 G. Xi, J. Ye, Q. Ma, N. Su, H. Bai, C. Wang, *J. Am. Chem. Soc.*, **2012**, *134* , 6508–6511.
7 S. Goel, Z. Wu, S. I. Zones, E. Iglesia, *J. Am. Chem. Soc.*, **2012**, *134*, 17688–17695.
8 H. Zhang, M. Jin, Y. Xia, *Angew. Chem. Int. Ed.*, **2012**, *51*, 7656-7673.
9 D. Wang, Y. Li, *Adv. Mater.*, **2011**, *23*, 1044-1060.
10 Z. Jin, F. Wang, F. Wang, J. Wang, J. C. Yu, J. Wang, *Adv. Funct. Mater.*, **2013**, *23*, 2137-2144.
11 T. K. Sau, A. L. Rogach, *Adv. Mater.*, **2010**, *22*, 1781-1804.
12 C. Wang, J. Fang, *ChemSusChem*, **2013**, *6*, 1848-1857.
13 S. Rawalekar, T. Mokari, *Adv. Energy Mater.*, **2013**, *3*, 12-27.
14 C. Y. Chiu, H. Wu, Z. Yao, F. Zhou, H. Zhang, V. Ozolins, Y. Huang, *J. Am. Chem. Soc.*, **2013**, *135*, 15489–15500.
15 B. T. Sneed, C. H. Kuo, C. N. Brodsky, C. K. Tsung, *J. Am. Chem. Soc.*, **2012**, *134*, 18417–18426.
16 C. Gao, Q. Zhang, Z. Lu, Y. Yin, *J. Am. Chem. Soc.*, **2011**, *133*, 19706–19709.
17 C. C. Lee, W. C. Ke, K. T. Chan, C. L. Lai, C. H. Hu, H. M. Lee, *Chem. Eur. J.*, **2007**, *13*, 582-591.
18 N. Kudo, M. Perseghini, G. C. Fu, *Angew. Chem., Int. Ed.*, **2006**, *45*, 1282-1284.
19 L. Mandeltort, D. L. Chen, W. A. Saidi, J. K. Johnson, M. W. Cole, J. T. Yates, Jr, *J. Am. Chem. Soc.*, **2013**, *135*, 7768–7776.
20 R. Liu, A. Sen, *J. Am. Chem. Soc.*, **2012**, *134*, 17505–17512.
21 C. Zlotea, R. Campesi, F. Cuevas, E. Leroy, P. Dibandjo, C. Volkringer, T. Loiseau, G. Férey, M. Latroche *J. Am. Chem. Soc.*, **2010**, *132*, 2991–2997.
22 T. Ishida, M. Haruta, *Angew. Chem. Int. Ed.*, **2007**, *46*, 7154-7156.
23 I. Washio, Y. Xiong, Y. Yin, Y. Xia, *Adv. Mater.*, **2006**, *18*, 1745–1749.
24 X. Xia, J. Zeng, L. K. Oetjen, Q. Li, Y. Xia, *J. Am. Chem. Soc.*, **2012**, *134*, 1793–1801.
25 H. Sun, J. He, J. Wang, S. Y. Zhang, C. Liu, T. Sritharan, S. Mhaisalkar, M. Y. Han, D. Wang, H. Chen, *J. Am. Chem. Soc.*, **2013**, *135*, 9099–9110.
26 H. Miyamura, R. Matsubara, Y.Miyazaki, S. Kobayashi, *Angew. Chem, Int. Ed.*, **2007**, *46*, 4151-4154.
27 C. J. Murphy, C. J. Orendorff, *Adv. Mater.*, **2005**, *17*, 2173-2177.

28 H. Wu, R. Hong, X. Wang, R. Arvizo, C. You, B. Samarrta, D. Patra, M. T. Tuominen, V. M. Rotello, *Adv. Mater.*, **2007**, *19*, 1383-1386.

29 S. Abraham, I. Kim, C. A. Batt, *Angew. Chem. Int. Ed.*, **2007**, *46*, 5720-5723.

30 J. Han, R. Chen, M. Wang, S. Lu, R. Guo, *Chem. Commun.*, **2013,** *49*, 11566-11568.

31 J. Han, Y. Liu, R. Guo, *J. Am. Chem. Soc.*, **2009**, *131*, 2060-2061.

32 J. Han, Y. Liu, R. Guo, *Adv. Funct. Mater.*, **2009**, *19*, 1112-1117.

33 X. Lu, W. Zhang, C. Wang, T. Wen, Y. Wei, *Prog. Polym. Sci.*, **2011**, *36*, 671−712.

34 J. Stejskal, I. Sapurina, M. Trchová, *Prog. Polym. Sci.*, **2010**, *35*, 1420−1481.

35 D. Li, J. Huang, R. B. Kaner, *Acc. Chem. Res.*, **2009**, *42*, 135−145.

36 J. Han, J. Dai, L. Li, P. Fang, R. Guo, *Langmuir*, **2011**, *27*, 2181-2187.

37 J. Han, L. Wang, R. Guo, *J. Mater. Chem.*, **2012**, *22*, 5932-5935.

38 J. Han, L. Li, R. Guo, *Macromolecules*, **2010**, *43*, 10636-10644.

39 J. Han, Y. Liu, L. Li, R. Guo, *Langmuir*, **2009**, *25*, 11054-11060.

40 T. Zhang, J. Ge, Y. Hu, Q. Zhang, S. Aloni, Y. Yin. *Angew. Chem. Int. Ed.*, **2008**, *47*, 5806-5811.

41 Q. Zhang, T. Zhang, J. Ge, Y. Yin, *Nano Lett.*, **2008**, *8*, 2867-2871.

42 J. Ge, Q. Zhang, T. Zhang, Y. Yin, *Angew. Chem. Int. Ed.*, **2008**, *47*, 8924-8928.

43 J. Wang, K. G. Neoh, E. T. Kang, *J. Colloid Interface Sci.*, **2001**, *239*, 78-86.

44 S. Xuan, Y. J. Wang, J. C. Yu, K. C. Leung, *Langmuir*, **2009**, *25*, 11835-11843.

45 Y. Deng, Y. Cai, Z. Sun, J. Liu, C. Liu, J. Wei, W. Li, C. Liu, Y. Wang, D. Zhao, *J. Am. Chem. Soc.*, **2010**, *132*, 8466-8473.

46 Y. Chen, H. Chen, J. Shi, *Adv. Mater.*, **2013**, *25*, 3144-3176.

47 M. Pérez-Lorenzo, B. Vaz, V. Salgueiriño, M. A. Correa-Duarte, *Chem. Eur. J.*, **2013**, *19*, 12196–12211.

48 L. Zhang, T. Wang, L. Li, C. Wang, Z. Su, J. Li, *Chem. Commun.*, **2012**, *48*, 8706-8708.

49 D. Niu, Z. Ma, Y. Li, J. Shi, *J. Am. Chem. Soc.*, **2010**, *132*, 15144–15147.

50 Q. Zhang, I. Lee, J. Ge, F. Zaera, Y. Yin, *Adv. Funct. Mater.*, **2010**, *20*, 2201-2214.

51 C. Graf, D. L. J. Vossen, A. Imhof, A. V Blaaderen, *Langmuir*, **2003**, *19*, 6693–6700.

52 E. T. Kang, K. G. Neoh, K. L. Tan, *Prog. Polym. Sci.*, **1998**, *23*, 277-324.

53 S. Guo, S. Dong, E. Wang, *Small*, **2009**, *5*, 1869–1876.

54 B. J. Gallon, R. W. Kojima, R. B. Kaner, P. L. Diaconescu, *Angew. Chem., Int. Ed.*, **2007**, *46*, 7251–7254.

55 R. J. Tseng, J. Huang, J. Ouyang, R. B. Kaner, Yang, Y. *Nano Lett.*, **2005**, *5*, 1077–1080.

56 J. Han, J. Dai, C. Zhou, R. Guo, *Polym. Chem.*, **2013**, *4*, 313-321.

57 J. Han, M. Wang, S. Cao, P. Fang, S. Lu, R. Chen, R. Guo, *J. Mater. Chem. A*, **2013**, *1*, 13197-13202.

58 J. Han, M. Wang, R. Chen, N. Han, R. Guo, *Chem. Commun.*, **2014**, *50*, DOI: 10.1039/c4cc01532k

59 M. Q. Yang, X. Pan, N. Zhang, Y. J. Xu, *CrystEngComm.*, **2013**, *15*, 6819-6828.

60 P. Hervés, M. Pérez-Lorenzo, L. M. Liz-Marzán, J. Dzubiella, Y. Lu, M. Ballauff, *Chem. Soc. Rev.*, **2012**, *41*, 5577-5587.